DOI: 10.13009/EUCASS2017-266

Localized micro-discharges group DBD vortex generators - disturbances source for active transition control

Moralev Ivan *, Bityurin Valentin *, Firsov Alexander*, Sherbakova Victoria**, Selivonin Igor**, Maxim Ustinov***

** Institute for High Temperatures RAS*

127415, Izhorskaya str. 13 bld.2Moscow, Russia,

*** Moscow Power Engineering Institute*

Krasnokazarmennaya str.17, Moscow, Russia

**** Central Aerohydrodynamic Institute,*

Zhukovsky str.1, Zhukovsky, Russia

morler@mail.ru

Abstract

New type of DBD plasma actuator for boundary layer control, based on the controllable inhomogenuity of the discharge along the exposed electrode, is developed. The structure of the flow, generated by the isolated groups of microdischarges, was studied in details in quiescent conditions. In the 2D laminar boundary layer the flow structure downstream of the actuator was studied at external flow velocities up to 7.5 m/s for various sweep angle of the electrode. The equivalent model of the actuator, including the force and heat sources, is formulated based on the analysis of the flow created by the actuator in quiescent conditions. The model is verified by simulating the flow downstream of the actuator in 2D boundary layer. As a final step, the applicability of the localized microdischarge group actuator for active transition control on a swept wing was studied. The generation of a cross-flow mode by the actuator was demonstrated in numerical simulation for low-velocity experiment conditions.

1. Introduction

Control of the laminar-turbulent transition is important from the point of view of aircraft drag reduction. At the moment, the development of wings with a laminar profile allows one to significantly shift the point of the transition downstream, obtaining a substantial gain in the wing quality at cruise conditions. At the same time, this solution works only on straight wings, where the transition in flight conditions is governed by the Tollmin-Schlichting waves development. At large sweep angles, the transition is triggered by the instability of the cross-flow profile, existing in the three-dimensional boundary layer on the wing surface.

At low-turbulence condition, stationary modes have the highest intensity in the boundary layer. Thus, the methods of delaying the transition on a swept wing are usually associated with the control of the development of these stationary modes. As one of the approaches, it was proposed to use the nonlinear interaction of the disturbances with different wavelength [1]. Short-wave stationary perturbations were introduced near the leading edge of the wing by mechanical discrete roughness elements; their development led to a decrease in the amplitude of the fundamental mode at the late stage of growth.

In recent works [2]–[5], plasma actuators based on a dielectric barrier discharge were considered as a source of such perturbations. These devices were introduced into the practice of aerodynamic experiment in the 90s; at the moment, their application has been considered in relation to many problems of aerodynamics and aeroacoustics [6]–[8]. The physics of actuators effect upon the flow is associated with the appearance of a bulk force in a decaying discharge plasma at the edge of the corona electrode, and also with volumetric heat release in the discharge channels. The excitation of the CF modes was demonstrated numerically with respect both to the conditions of the low-speed experiment [2] and real subsonic cruise flight conditions [3] . Recently, there are also experimental studies confirming the possibility of using plasma actuators to excite CF modes [5].

It is worth noting that the models of heat sources and volumetric force used in these works are of a rather arbitrary nature; they are based on the extrapolation of data from various experimental groups. The most critical drawbacks of these models are the use of two-dimensional sources of volume force, as well as ignoring the processes of heat release in the discharge. It should be noted that the structure of the volume force in the discharge is determined by the distribution of the electric field, which is significantly affected by the charge deposited on the surface of the

DOI: 10.13009/EUCASS2017-266

dielectric. In this connection, the force created by a single microdischarge is always three-dimensional; the two-dimensional flow at the edge appears as a result of addition of perturbations from individual microdischarges, whose position is arbitrary at large amplitudes of the supply voltage. At a limited width of the plasma formation region, no compensation of the transverse component of the force occurs at its edges. This eventually leads to the complex structure in the flow structure created by such a narrow group of microdischarges in still air and the boundary layer [9], [10].
This work is devoted to the development and investigation of plasma actuators for active control of the transition on the swept wing. The design of the actuator is based on the "sandwich" configuration, in which the position of the microdischarge groups is controlled by the construction of the underlying electrode. The perturbations generated by an actuator in quiescent air and in a low-velocity 2D boundary layer are studied. Based on the analysis of flow in quiescent conditions, a semiempirical simplified model of the actuator is developed, which is then verified on the structure of the vortices that appear behind the actuator in the boundary layer. Using the proposed model, the modeling of the CF mode generation in a three-dimensional boundary layer was carried out.

2. Experimental details

To predefine the spanwise structure of the discharge, the sandwich-type actuator design was used. Actuator design is shown in Figure 1a. Buried electrode was made in two layers: lower one was solid and upper one (control electrode) was composed of equidistantly arranged metallic strips. The distance between the strips was 4 mm. The two layers were electrically connected. For both actuator types, alumina ceramics with dielectric strength ε~10 was used as a dielectric. The exposed electrode was made of 20μm copper foil.

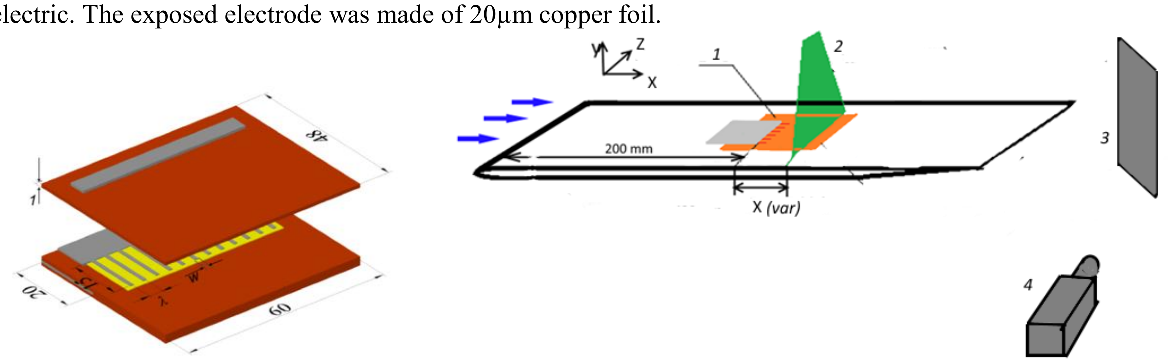

Figure 1 a) Design of the sandwich plasma actuator for LMDGs formation. b) Schematic diagram of experimental arrangement for the visualization of longitudinal vortices in boundary layer downstream the discharge: 1- plasma actuator,2- laser sheet; 3- mirror; 4- camera.

The discharge was powered by a transistor high-frequency generator with resonance output filter. The voltage amplitude on the discharge gap was varied within U = 2–4 kV and the frequency of f = 150-200 kHz.
The flow in the boundary layer around actuator was experimentally studied in a D-2 wind tunnel of the Institute for High Temperatures RAS (Moscow). This open-type setup has an octahedral test section with dimensions 100 x 100 x 600 mm and nozzle constriction ratio of 1:16. The turbulence level was reduced by honeycomb and fine-mesh grid mounted in front of the nozzle. The turbulence level in the freestream at 30 m/s was below 0.2%. The boundary layer was formed on a flat plate with dimensions 20 x 100 x 8 mm, which was set at a zero angle of attack. The front edge of the plate had a super-elliptical shape with 8:1 elliptic ratio. The rear edge was cut at 6 deg angle in order to eliminate flow separation. The plasma actuator was positioned at a distance of about 200 from the front edge and mounted flush with the plate surface. The experiments were performed at an airflow velocity of 7.5 m/s, providing the boundary layer thickness at the actuator position δ_{99}= 3.3 mm (δ_{ref}= 0.67 mm).
The flow structure downstream of the actuator was studied using a particle image velocimetry (PIV) system. The measurements were performed in a plane perpendicular to the flow direction (Figure 1a). In order to minimize the error of the transverse velocity components caused by perspective distortions, the camera view direction was selected normal to the observation plane. The image was obtained with the aid of a 30x 50 mm mirror oriented at 45 deg relative to the flow axis and placed at a distance above 100 mm from rear edge of the plate. The image of particles was processed using a cross-correlation algorithm with 32x32 px window, 75% overlap, and vectors filtering by the S/N criterion at the postprocessing stage. A single velocity field in a selected plane was obtained by averaging over 70 instantaneous flow patterns. The flowfield resolution in the laser image plane was 100x100 μm. A 3D field of two velocity components was obtained by shifting the object at 0.5–1 mm step in the plane perpendicular to the laser

DOI: 10.13009/EUCASS2017-266

sheet. The flow was seeded with TiO2 particles with diameters within 0.1–1 μm, which were introduced into the wind tunnel in a forechamber before the honeycomb.

2. Results

2.1 Actuator-induced flow in quiescent conditions

The structure of the flow induced by the discharge in sandwich actuator in the absence of an external flow was investigated using stereo-PIV. It can be seen (Figure 2) that each group of microdischarges localized above the control electrode generates a wall jet near directed away from the edge of the exposed electrode. In addition, on the edge of each group, there are two regions where fluid moves along the electrode edge. Farther from the electrode, these regions are folded into a pair of longitudinal vortices with the opposite rotation direction. Jet momentum redistribution by these vortices leads to the shift of the velocity maximum to the region between the positions of the MD groups. Since the distance between the vortices is sufficiently small, a vortex pair is advected away from the surface of the dielectric, which in turn leads to an increase in the wall jet thickness.

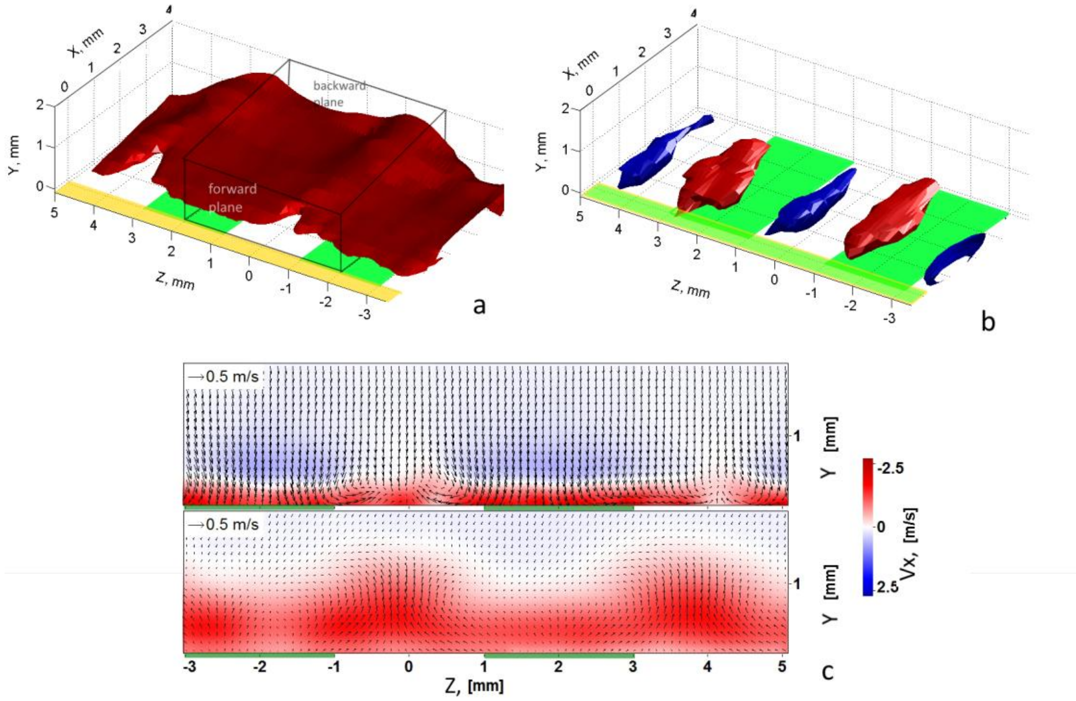

Figure 2 a) u isosurface with a control box for the total force estimation b) Isosurfaces of the longitudinal vorticity, c) Velocity fields in the YZ planes. Control electrodes positions are marked by green.

2.2 Flow induced by the actuator in the boundary layer

0 deg sweep angle

When the flow is normal to the electrode edge, the flow structure in the downstream boundary layer was found to be strongly affected by the 3D force distribution at the edge of the discharge formation regions. It is shown (Figure 3) that the single actuator section generates a pair of counter-rotating longitudinal vortices with the flow velocity in the core up to 0.5 m/s and core diameter on the order of 1 mm. The formation of a constricted channel leads to the significant increase of the vortices intensity.

When the actuator with periodical spacing of the electrode sections is used, an array of vortices is formed in the downstream boundary layer. The circulation in the vortex cores is increased only along the discharge region, switching downstream to the viscous dissipation. The dissipation rate is strongly affected by the liftoff of the vortex pairs from the surface.

30 deg sweep angle

DOI: 10.13009/EUCASS2017-266

In the case when the electrode sweep angle to the oncoming flow is not zero, the role of the longitudinal (normal to electrode edge) force increases. As can be seen in Figure 4, in the downstream boundary layer the flow consists of an array of the co-rotating vortex filaments. The peak velocity in the vortex cores is up to 1m/s.

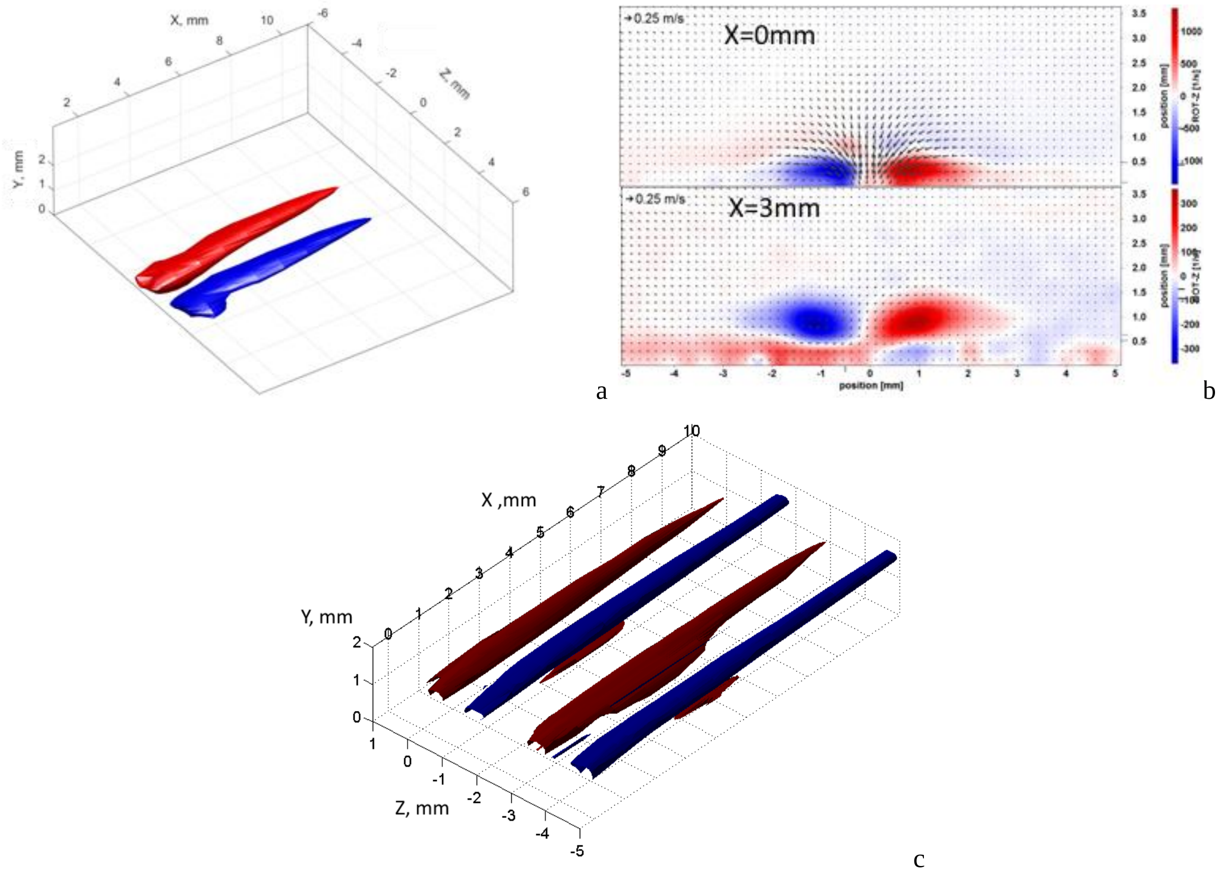

Figure 3 Longitudinal vorticity contours downstream of the actuator location. a,b) Single section, U=3.6kV, c)Array with 4mm step, U=3.2kV,

DOI: 10.13009/EUCASS2017-266

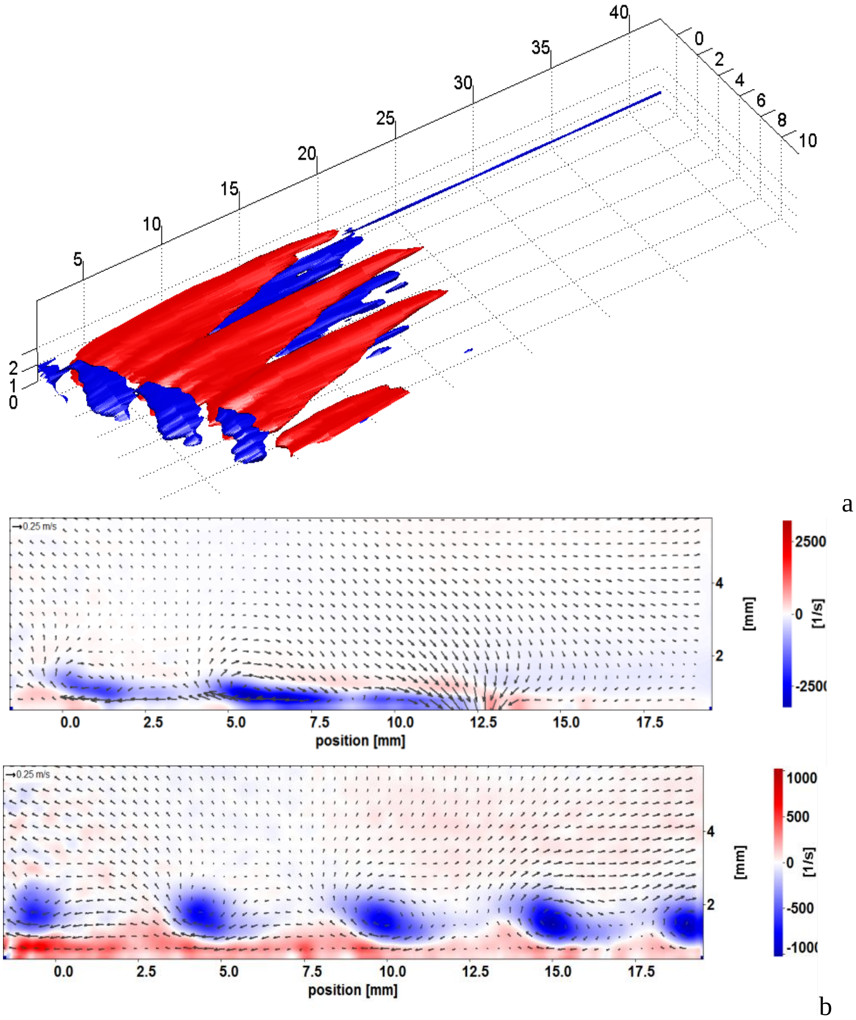

Figure 4 a) Longitudinal vorticity isosurface in the boundary layer downstream of the discharge b) cross-sections of the flow for increasing X position Color represents inverted longitudinal vorticity.

2.3 Actuator numerical model formulation

To provide the estimation of the effectiveness of CF modes generation by LMDG actuator, the equivalent model was developed. The model was developed on the base of the flow structure measurements in quiescent conditions and then verified by the experiments in 2D boundary layer. Principal scheme of the equivalent source is given in fig. One can see that the actuator is replaced by the pair of regions, symmetrical towards the central plane. Inside the regions, the heat release density and three force components are given. For simplicity, only two force components: f_x and f_z are considered; wall-normal force is set to be zero. For the preliminary estimation, the heat release and forcing region were set identical, with the dimensions (l, w, h). Therefore, to fully determine the source one should set 6 parameters: geometry (l, w, h), force density (f_x , f_z) and heating density q:These parameters were partly obtained from the experiment, partly chosen to fit quiescent conditions test. From the experiment there were determined the total heat release, the integral longitudinal force and the approximate geometry of the forcing region. The remaining parameters: tangential force amplitude and structure were obtained from the modelling. The description of the procedures used is given below.

Longitudinal force, F_x

Estimation of the X-component of the EHD force, generated by the discharge, was performed on the basis of the analysis of the integral momentum balance. Momentum fluxes were estimated on the surface of the box (see Figure 2), encircling two half-sections of the actuator.

The total volume force acting upon the gas inside the box can be estimated as

DOI: 10.13009/EUCASS2017-266

$$F_z = \int_{forw}(p + \rho V_x^{\ 2})dzdy - \int_{back}(p + \rho V_x^{\ 2})dzdy + \rho \int_{top} V_x V_y dxdz + \int_{wall} \tau_w dxdz \quad \textbf{(1)}$$

For the estimation, the effect of the pressure distribution and viscous friction can be neglected, thus provided the box size is enough, we can write

$$F_x = \int_{forw} \rho V_x^{\ 2} dzdy - \int_{back} \rho V_x^{\ 2} dzdy \qquad \textbf{(2)}$$

Omitting viscous term leads to the underestimation of the force by approximately 20%, that is acceptable at this step. Total force in the longitudinal direction, generated by the actuator for the studied conditions (U=3.2 kV, f=190 kHz, λ=4 mm, w=2 mm), is estimated as F_x=5 10^{-6} N. Corresponding linear force density is f_{zl}=2.5 10^{-3} N/m, that exactly corresponds to the analytical approximation. Finally, estimation of the force density is f_z=8.3 10^3 N/m^3.

Forcing volume

To determine the forcing volume, we have analyzed the initial stage of the flow acceleration. It was shown that on the acceleration stage, a 3D starting vortex is formed near the actuator. During first stages (~0.5 ms) the convection term in the Navies-Stokes equations can be neglected and then the acceleration in the flow is due to the volumetric force and pressure gradient [12].The developing flowfield in the central plane was analyzed (Figure 5), in terms to avoid the interference of the 3D force and pressure gradient. In this case, the domain of flow acceleration in positive direction can be interpreted as a forcing region. The resulting dimensions of the forcing region in XY plane is 1.5x0.2 mm. One should note that elongation of the source in X direction is in agreement with the length of the discharge for the tested conditions. In transverse direction the size of the forcing region was chosen to be equal to the section width (2 mm).

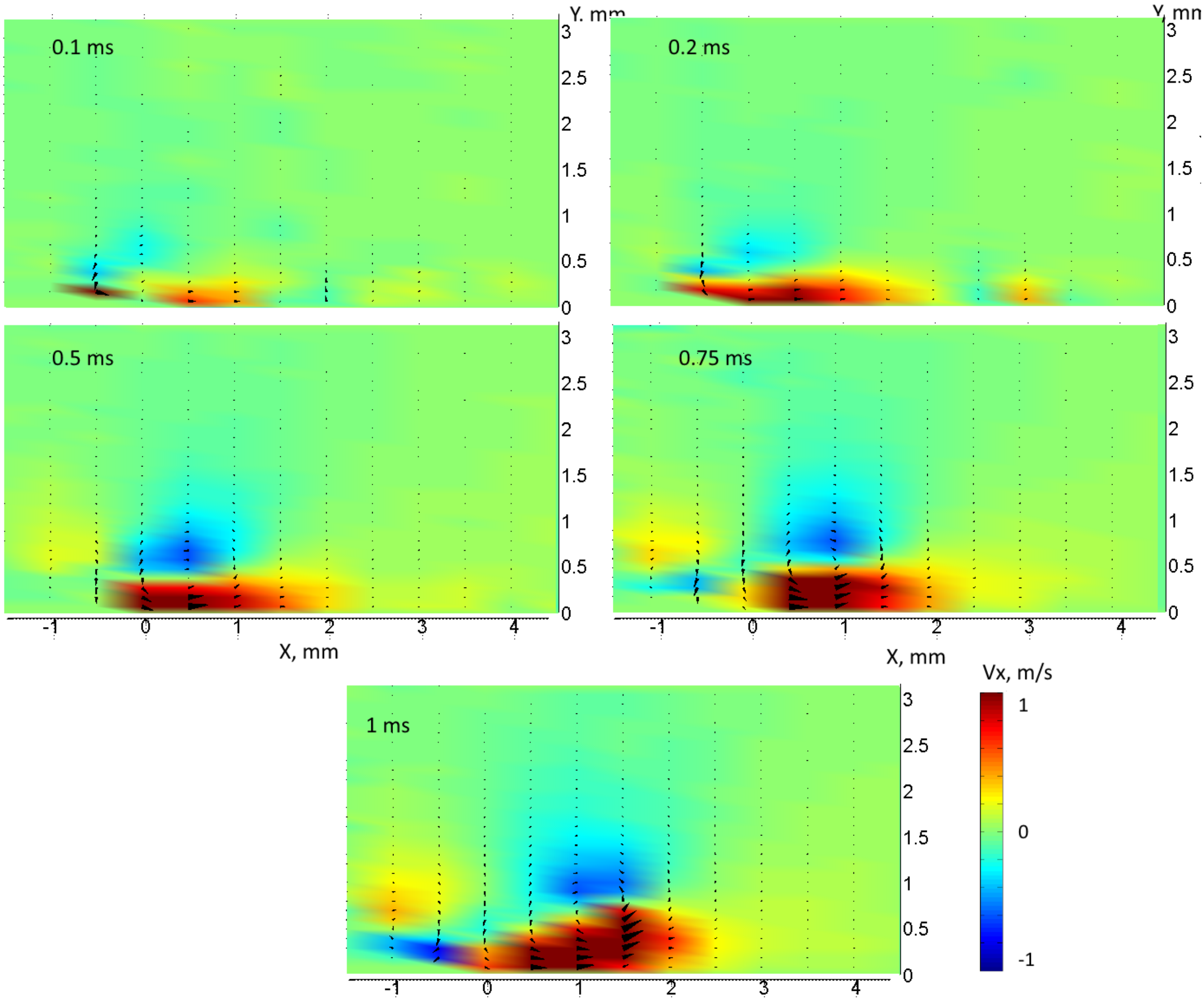

Figure 5. Flow dynamics at central cross-section after the start of the HV pulse. a- 0.2ms, b-0.5ms

DOI: 10.13009/EUCASS2017-266

Transversal force component f_z

The value of the transversal force component was chosen to fit the flow structure at quiescent conditions. A series of computations was performed, varying the f_z transverse force density from 0 to 100% of the f_x. One can see (Figure 6) that transversal component of the force should be taken into account to fit the obtained velocity distribution in the wall jet, induced by actuator. The best fit was observed for f_z~0.5 f_x.

Finally, the model of a single section of the actuator was formulated as follows:

The section (Figure 7) is presented as two symmetrical domains with the characteristic size of LxHxW=1.5x0.2x1 mm. Inside the domains, the homogeneous heat source and volumetric force are determined. The direction of the tangential force component inside the half-sections is opposite, while the longitudinal one is similar. The heat and force sources are described as

- Total longitudinal force (exp) F_x=2.5e-6 N ; Force density f_x=8e3 N/m^3
- Tangential force F_z=1.2e-6 N; Force density f_z=~4e3 N/m^3
- Total heat release Q=0.3 W ; Heat release density q=1e9 W/m^3

All integral values are given for half-sections. The model was formulated for the supply voltage amplitude of 3.2 kV and frequency 190kHz. For other frequencies, both force and heat release terms were scaled proportionally with frequency.

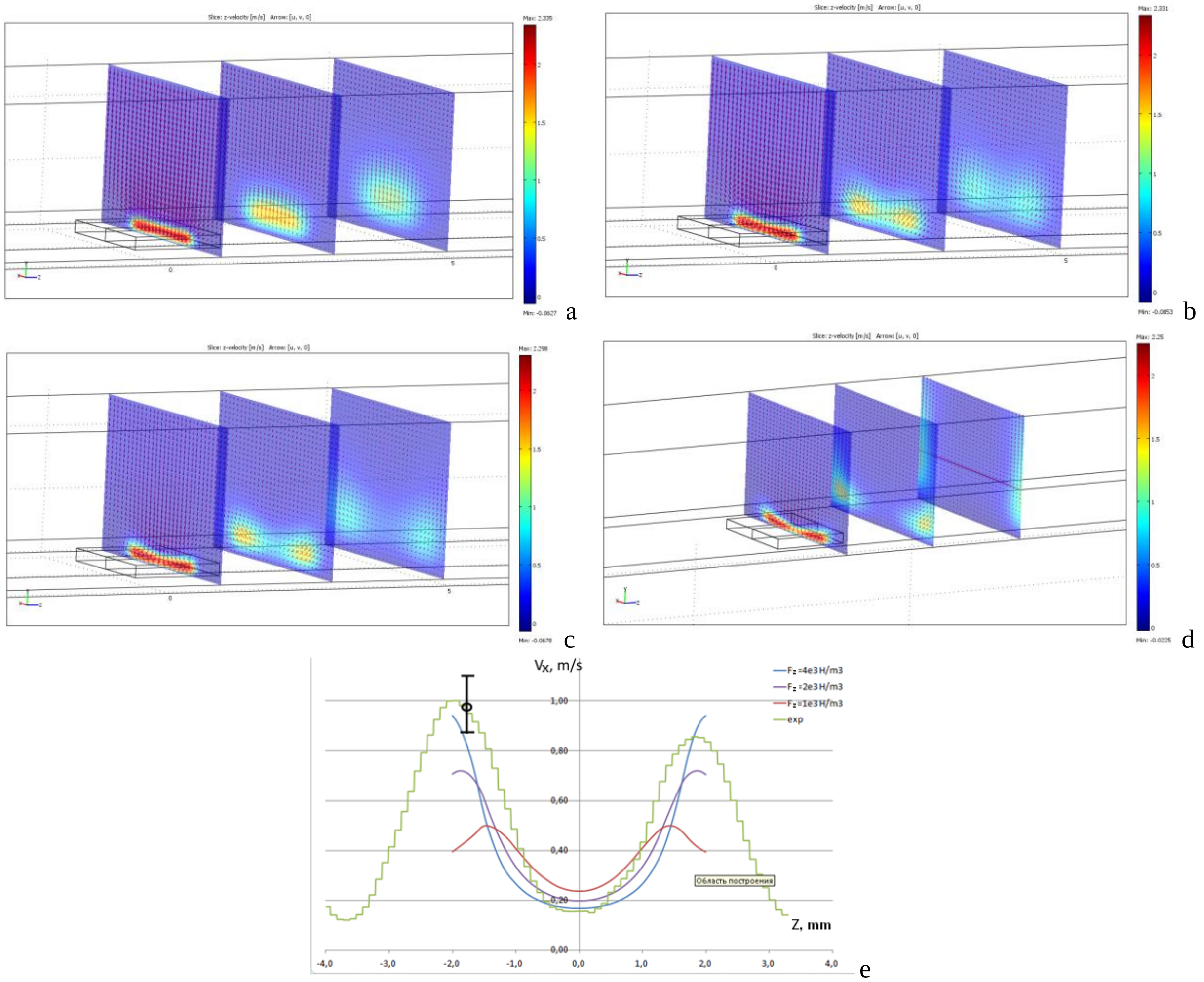

Figure 6. Modeling of the flow in quiescent conditions at various transversal force component a) f_z=0, b) f_z=1e3N/m^3 c) f_z=2e3N/m^3 d) f_z=5e3N/m^3. f_x=8e3 N/m^3, fy=0, q=0, e) longitudinal velocity profiles along the line at (X,Y)=(5,1). Smooth curves- calculation results for cases a-d, stepwise- experimental data

DOI: 10.13009/EUCASS2017-266

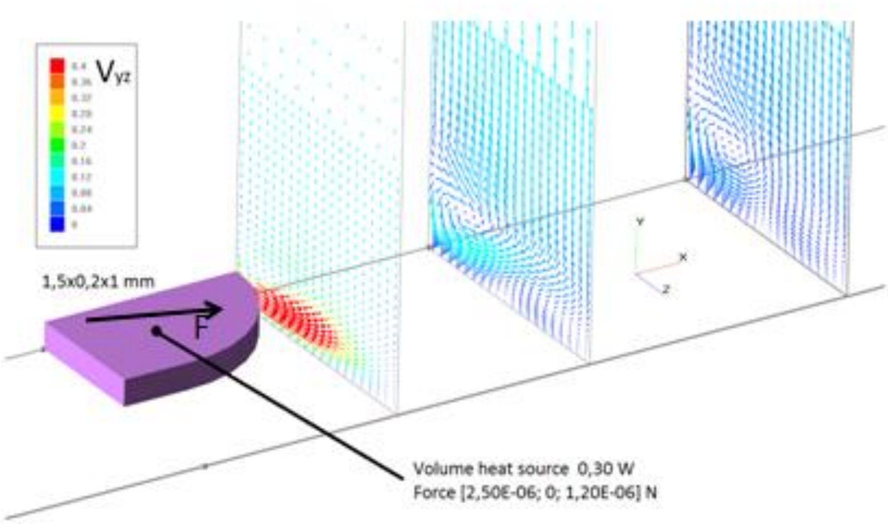

Figure 7. Half- model of the actuator section. Left XY plane is a symmetry plane, ZX is a streamlined surface. Sections are "attached" to the exposed electrode with a predefined spanwise wavelength.

2.4 Modeling of the flow downstream of the actuator

Sweep angle 0 deg

Flow structure downstream of the actuator section was calculated using FlowVision CFD software for the conditions of the boundary layer experiment: V=7.5m/s, δ=3.3mm. In the calculation, the actuator model described in previous section was used; all values were scaled down by a factor of 0.75 to take into account the lower supply frequency in the boundary layer experiment.

Figure 8 represents the longitudinal vorticity fields in the consequent cross-sections downstream of the actuator. Left image represents data obtained from the experiment, right ones- from numerical modeling. Additionally, curves in Figure 8b represents the evolution of the circulation Γ of the longitudinal vortex as a function of distance to the actuator. The latter was calculated by following procedure. In x-vorticity field at certain YZ plane, all values below 10% of the maximum value in the vortex core were set to zero; after that, ω_x was integrated over the certain plane. For the experimental data, the final result was averaged over all vortices in the measured flowfield.

The qualitative agreement can be seen; however, detailed analysis finds some discrepancies. Modeling results shows that a pair of longitudinal vortices are formed downstream of the actuator section. One can see that the amplitude of the vortices is somehow overestimated. Vortices trajectory calculated on the basis of the equivalent model are different from the ones found from the experiment. In the experiment, vortices seem to be more concentrated and are lifted above the surface. The other discrepancy can be found in the vortex dissipation rate as can be seen in Figure 8b. The model overpredicts the dissipation rate, at least at relatively short distances from the actuator. One can assume that this discrepancy is the result of different vortex geometry and distance to surface. The other possible reason of the overestimation of the vortex dissipation is numerical approximation errors, present in the numerical scheme of the FlowVision solver.

The source of these discrepancies obviously lies in more or less arbitrary distribution of the lateral force component over the discharge volume. Higher force densities, concentrated about the edge of the discharge regions, will lead to more concentrates vortex cores, more intense vortex liftoff, and hence the lower dissipation rates.

DOI: 10.13009/EUCASS2017-266

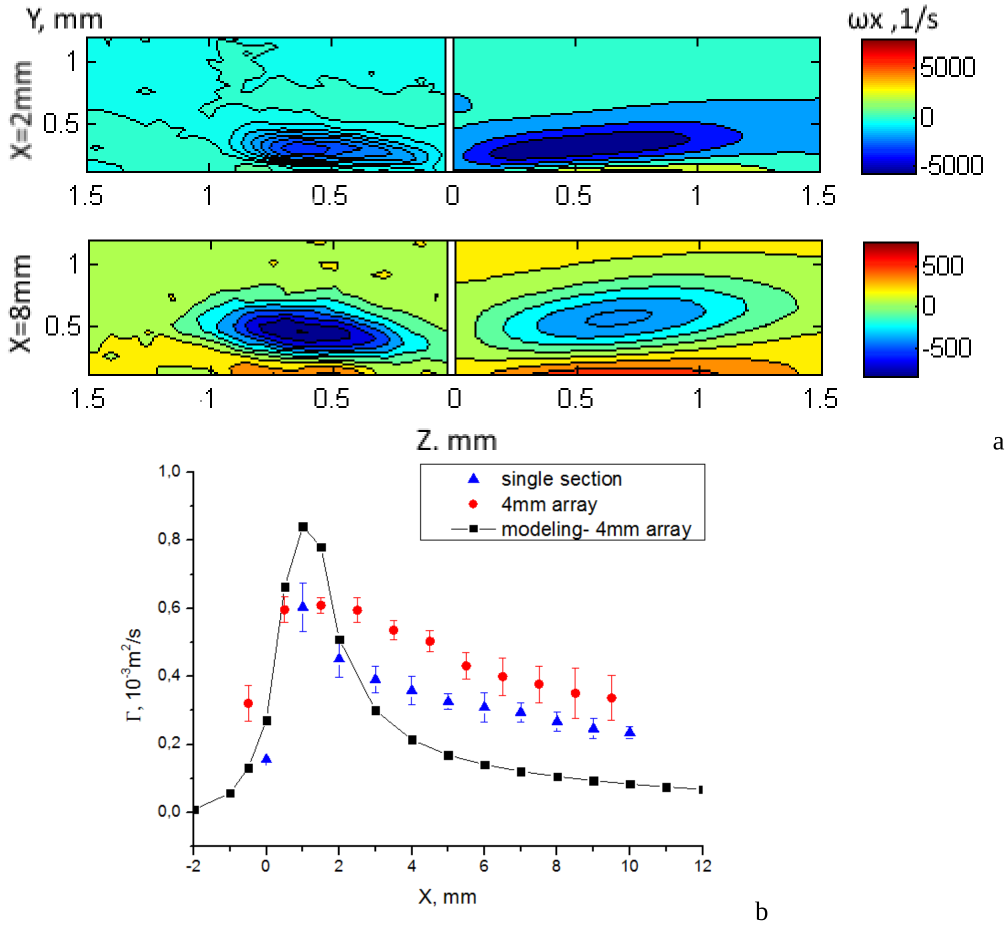

Figure 8. Comparison of the calculated and experimentallt obtained vortices structure and intensity for 0 deg sweep angle of actuator. a) Experimental (left) and modeled (right, z axis mirrored) longitudinal vorticity distribution in cross-flow planes. 4mm step array of actuators b) Circulation evolution in flow direction.

Sweep angle 30 deg

The same calculations were performed for the 30 degrees sweep angle of the actuator section. The comparison of the experimentally obtained and modelled flowfields are shown in Figure 9a; Figure 9b presents the evolution of the vortex circulation along the flow direction. Again, one can see that the model qualitatively well predicts the structure of the induced flowfield, as well as an initial vortex amplitude. Anyhow, the modelling shows lower position of the vortex cores and the dissipation rate is overpredicted for small distances from the actuator.

DOI: 10.13009/EUCASS2017-266

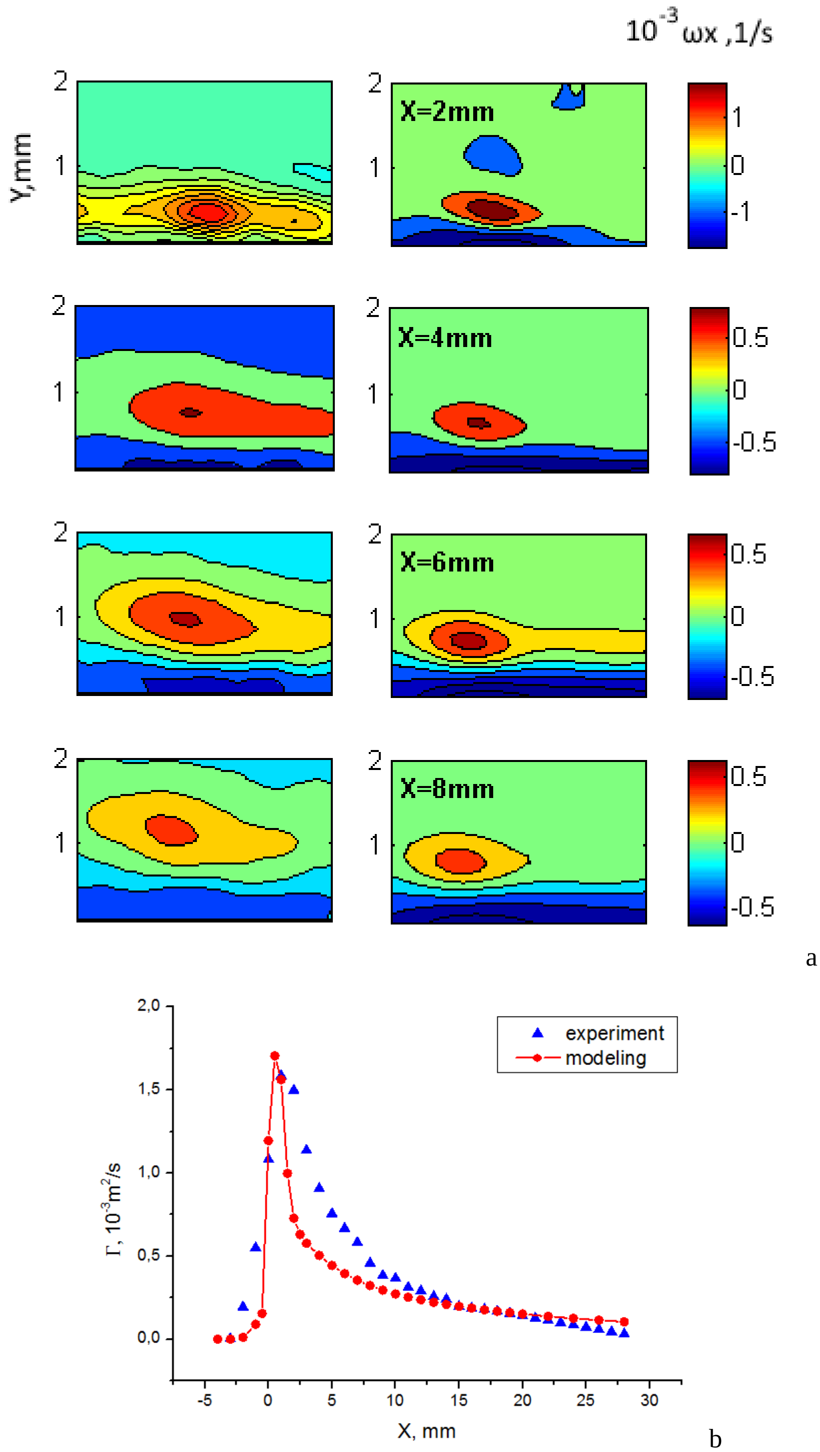

Figure 9. Comparison of the calculated and experimentallt obtained vortices structure and intensity for 30 deg sweep angle of actuator. a) Experimental (left) and modeled (right) longitudinal vorticity distribution in cross-flow planes. 4mm step array of actuators b) Circulation evolution in flow direction.

2.5. Estimation of amplitude of cross-flow instability mode generated by LMDG plasma actuator

One of prospective methods of swept-wing laminar-turbulent transition delay is production of artificial short-period steady cross-flow instability modes (“killer modes”) which change the velocity profile in the boundary layer and retards growth of the dominated mode of larger period which is responsible for transition. Initially these “killer modes” were generated by discrete roughness elements (DRE) located near the leading edge [1]. Usage of DBD actuators instead of roughness elements is preferable because of this eludes to change amplitude and period of “killer

DOI: 10.13009/EUCASS2017-266

mode”. In this section the feasibility of designed LMDG actuator for such control of cross-flow dominated transition is estimated. For this purpose the amplitude of steady “killer” mode generated by body force sources found in section 3 is computed for the conditions of planned experiment in low-speed wind tunnel T-124 of TsAGI. The experiment will be performed with the special model for realization of three-dimensional boundary layer at the flat plate shown in Figure 10. It consists from four general parts: inserts mounted at the upper and side walls (denoted by 1, 2, 3 in Figure) and plate with swept leading edge 4. The sweep angle of upper displacement body and the leading edge of the plate equal to 35^0. The pressure distribution at the upper side of the plate is similar to this at the forward part of the upper surface of the swept wing with the same sweep angle. Exposed electrode of LMDG actuator will be directed parallel to the leading edge and located at distance $x'=130$ mm from it. Period of micro-discharges produced by this actuator $d'=50mm$ is equal to the period of “killer” mode. The measurements will be performed for flow velocity in the range 30-40m/s. Amplitude of generated “killer” mode is computed for maximal flow velocity 40m/s.

(a) (b)

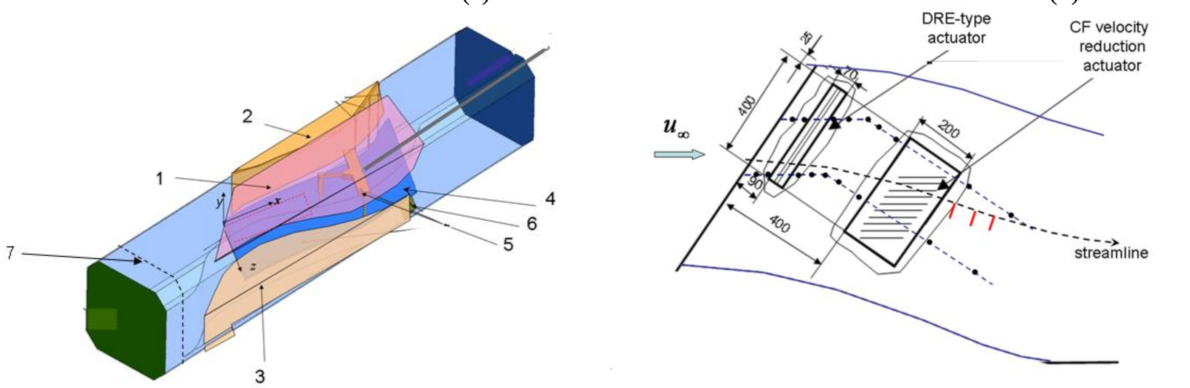

Figure 10. a) General view of the model in the test section. b) Design of the plate for investigation of transition control by DBD actuators

Effect of discharge on the flow can be modeled by a spanwise-periodic sequence of body forces $\vec{F}'$ concentrated in each micro discharge location at the trailing edge of exposed electrode. These forces have longitudinal $\vec{F}'_x$ and spanwise $\vec{F}'_z$ components. Air heating by discharge is rather weak and flow velocity is assumed to be small with respect speed of sound, so model of incompressible fluid with constant density and viscosity will be used further. Non-dimensional variables are introduced using boundary layer thickness $\delta'=(\nu L'/u_\infty)^{1/2}$ and free-stream velocity u_∞ as scales. Non-dimensional discharge induced forces are introduced as $F=F'/(\rho u_\infty^2\delta')$. Chord of the model in this experiment will be 1m, free-stream velocity $u_\infty=40m/s$, boundary layer thickness $\delta'=(\nu L'/u_\infty)^{1/2}$~0.6mm. Following analytical approximation for longitudinal and spanwise components of non-dimensional body force were used here

$$F_x=A_x\theta(\bar{x})\frac{\bar{x}\bar{y}}{2\sqrt{\pi}}e^{-(\bar{x}+\bar{z}^2/4+\bar{y})};\quad F_z=A_z\theta(\bar{x})\bar{x}\bar{y}\bar{z}e^{-(\bar{x}+\bar{y}+\bar{z})};\quad \bar{x}=x/x_0,\quad \bar{y}=y/y_0,\quad \bar{z}=z/z_0 \quad \textbf{(3)}$$

where $x_0=l_x'/\delta,\ \ y_0=l_y'/\delta,\ \ z_0=l_z'/\delta$ - non-dimensional coordinates of force maximum, $l_x'=0.75mm,\ \ l_z'=0.5mm,\ \ l_y'=0.1mm,$ - dimensional coordinates of this maximum defined as a half of corresponding sizes of force box fined in section 2.3, $\theta(\bar{x})$ - Heaviside function. Amplitudes A_x, A_z were chosen to obtain experimental integral values of dimensional force components $F_{x\Sigma}=5\times10^{-6}N,\ \ F_{z\Sigma}=1.2\times10^{-6}N$. These distributions of streamwise and spanwise components of non-dimensional force in maximum over z are shown in Figure 11. To find dimensional body force densities these distributions should be multiplied by factor $\rho u_\infty/\delta\sim6\times10^6$ [N/m^3]. This gives maximal densities of streamwise and spanwise componemts of discharge-induced force $F_x'\sim10^4N/m^3$, $F_z'\sim3\times10^3N/m^3$ which are close to estimates found in section 2.3. One should note that in this section, Z and Y axes are interchanged.

DOI: 10.13009/EUCASS2017-266

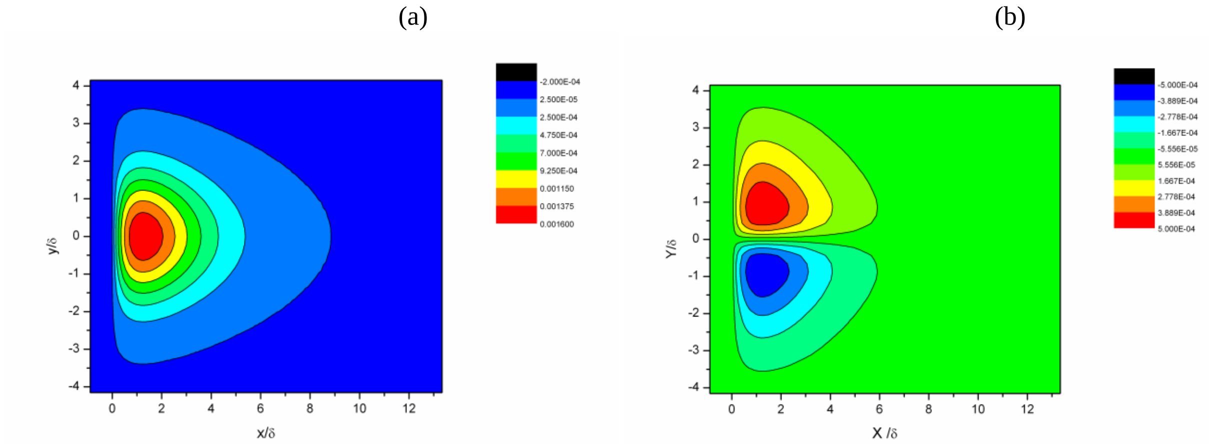

Figure 11 Distributions of longitudinal (a) and spanwise (b) components of non-dimensional body force induced by micro-discharge used for estimation of amplitude of generated "killer" mode

Solution for velocity vector $\mathbf{V}$ in the vicinity of the actuator will be sought as a sum of two terms:

$$\mathbf{V}(x,y,z)=\mathbf{V}_0(y)+\varepsilon\mathbf{v}_p(x,y,z) \qquad \textbf{(4)}$$

The first one corresponds to undisturbed boundary layer which is assumed to be uniform over *x* and *z*. The second term describes three-dimensional small-amplitude perturbations excited by discharge. Folkner-Scan-Cook self-similar solution for profiles of longitudinal U_0 and spanwise V_0 velocity

$$\begin{aligned}
&U_0=\left(\frac{x'}{L'}\right)^m f'(\eta)\cos\chi; \quad V_0=g'(\eta)\sin\chi \\
&\eta=\frac{z\sqrt{m\cos\chi}}{\sqrt{\beta}\,(x'/L')^{\frac{1-m}{2}}}; \quad \beta=\frac{2m}{m+1} \\
&f'''+ff''+\beta(1-f'^2)=0; \quad f(0)=f'(0)=0; \quad f'(\infty)=1 \\
&g'''+fg''=0; \quad g(0)=g'(0)=0; \quad g'(\infty)=1
\end{aligned} \qquad \textbf{(5)}$$

with m=0.29 was used as a model of base flow in the boundary layer. It well approximates swept-wing boundary layer in the region of strong cross-flow instability. This solution in the actuator's location $x'=0.13\text{m}$ was used as the base flow $\mathbf{V}_0(y)$.

The perturbations are assumed to be periodic in *z*. Initially we shall assume that they die out for infinite *x*. This is true for subcritical case when the boundary layer is stable with respect to steady modes. Method of solution finding for growing modes generation will be discussed later. Assumptions made permit us to find solution for perturbations in form of combinations of Fourier series in *z* and Fourier integral in *x*.

$$\{\mathbf{v}_p\}=\sum_{n=-N}^{N}\frac{1}{\sqrt{2\pi}}\int_{-\infty}^{+\infty}\{\hat{\mathbf{v}}_n\}(k,z)e^{i(kx+\beta_n z)}dk \qquad \textbf{(6)}$$

where k and $\beta_n=2\pi n/d$ are wavenumbers in streamwise and spanwise directions. Substitution of (4),(6) into Navier-Stokes equations results in two infinite sets of Orr-Sommerfeld and Squire equations for Fourier transform of harmonics of perturbational velocity $\mathbf{v}_n$:

DOI: 10.13009/EUCASS2017-266

$$
\begin{aligned}
& i(kU_0+\beta V_o-\omega)(\hat{w}_n''-\gamma^2\hat{w}_n)-i(kU_0''+\beta_n V_o'')\hat{w}_n=\frac{1}{R}\left(\hat{w}_n^{IV}-2\gamma^2 w_n''+\gamma^4\hat{w}_n\right)+\\
& i\left(k\hat{F}_{xn}+\beta_n\hat{F}_{yn}\right)'\\
& i(kU_0+\beta_n V_o-\omega)\hat{\eta}_n+i(\beta_n U_0'-kV_o')\hat{w}_n=\frac{1}{R}\left(\hat{\eta}_n''-\gamma^2\hat{\eta}_n\right)+i\left(\beta_n\hat{F}_{xn}-k\hat{F}_{yn}\right)\\
& \hat{w}_n(0)=\hat{w}'_n(0)=\hat{\eta}_j(0)=0\,;\quad \hat{w}_n,\hat{\eta}_n\to 0\,;\, z\to\infty
\end{aligned}
\tag{7}
$$

In these equations $\hat{u}_n, \hat{v}_n, \hat{w}_n$, $\hat{F}_{xn}, \hat{F}_{xn}$ are components of Fourier transforms of harmonics of perturbational velocity and body force, $\hat{\eta}_n = i\beta_n\hat{u}_n - ik\hat{v}_n$ - are Fourier transforms of vertical vorticity, $R = u_\infty\delta/\nu$ - is Reynolds number. Equations (7) were solved for each value of *k* by matrix method based on collocation technique. In the unstable range of spanwise wavenumbers β_n solution found by Fourier transform method describe growing cross-flow instability mode originating upstream and cancelled by the force source. Appearance of such "strange" solution is caused by necessary to satisfy zero boundary conditions for $x \to \pm\infty$. Similar behaviour of growing TS wave generated by vibrator was obtained in [13]. To find the physically relevant solution describing generation of cross-flow instability mode by force, in accordance with principle introduced in [13], it is necessary to add to solution obtained from inverse Fourier transform the eigensolution of some amplitude. The amplitude of added eigenmode was found from the condition of vanishing of modified solution for $x \to -\infty$. Solution in the physical space was found by fast Fourier transform method.

(a) (b)

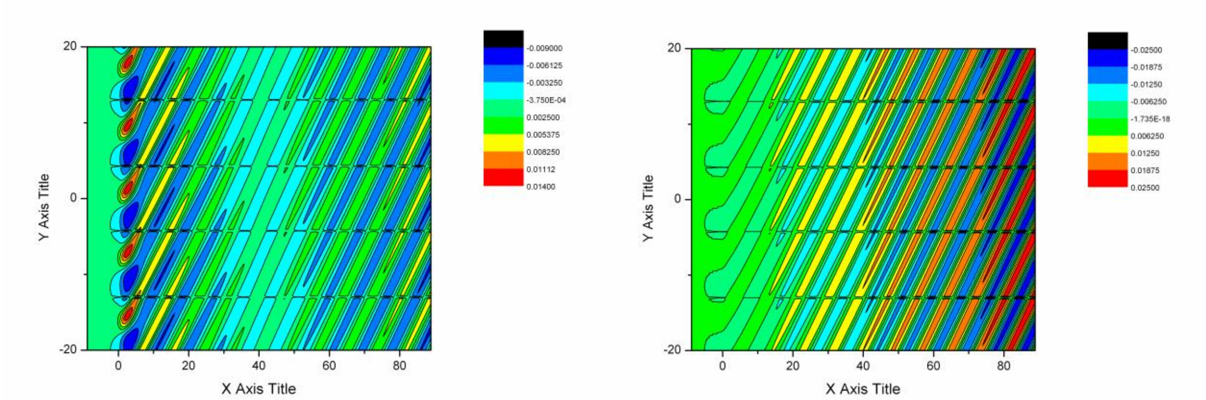

Figure 12. Distributions of tangential (parallel to the external streamline) component of perturbational velocity induced by micro-discharge actuator. (a) for z=0.2 (0.12mm), (b) for z=1 (0.6mm)

Distribution of perturbations of tangential velocity induced by actuator in *x,z* plane computed by described method is shown in Figure 12. At the small distance from wall y=0.12mm corresponding to maximum of body forces the local maxima of perturbations at the sides of micro-discharges appear. It is important that velocity perturbations here are well below of the level 10-13% which can initiate bypass transition. Further downstream the perturbations attenuate and their growth renews at the end of the computational region. Disturbances at large distance from the wall *z=0.6mm* corresponding to the maximum of tangential velocity profile of cross-flow instability mode generated demonstrate permanent growth. The evolution of these disturbances is better seen at Figure 13 where the perturbations of tangential velocity at *z=0.6mm* and y=*0* are plotted against *x*. Periodicity of disturbances over x well seen from the plot in linear scale at Figure 13 a and similar data plotted in logarithmic scale in Figure 13 b demonstrate exponential growth of perturbations. Initial amplitude of tangential velocity perturbations at the location of actuator is estimated from Figure 13 b as 1% from free-stream velocity. Computations of amplification curves of steady modes performed in the framework of linear stability theory (LST) for conditions of planned experiment in T-124 gave maximal N-factor of "killer" mode of period 5mm near 4. So, this mode generated by LMDG actuator should reach amplitude $0.01e^4$~1. In real flow the growth of this mode will be retarded by non-linear effects, but estimate based on LST demonstrates sufficient potential of its amplification which seems to be enough for laminar-turbulent transition control.

DOI: 10.13009/EUCASS2017-266

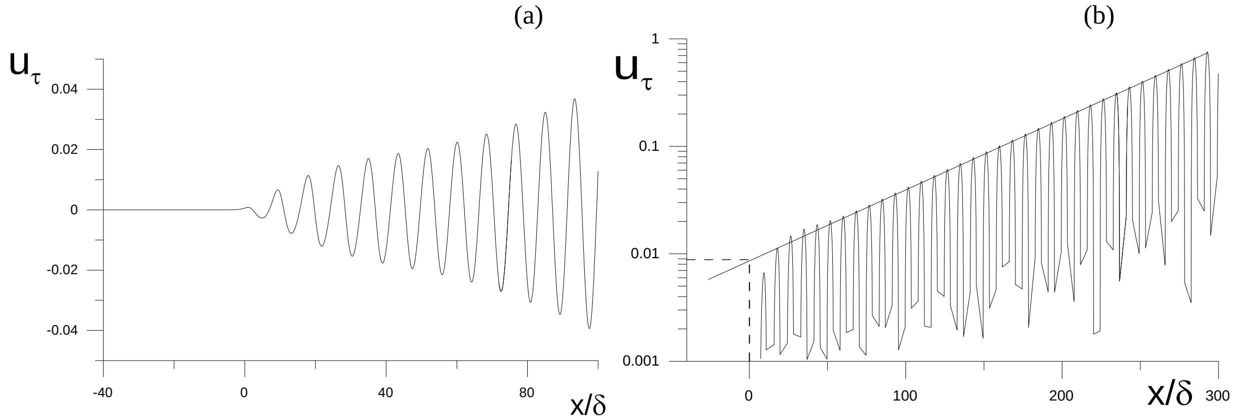

Figure 13. Perturbations of tangential velocity induced by micro-discharge actuator at y=0, z=1 as function of x. (a) –in linear scale, (b) – in logarithmic scale

3. Conclusions

The flow structure, induced by localized microdischarges group actuator (LDMG) was studied in the quiescent conditions and in a 2D boundary layer. It is shown that this actuator can create a longitudinal vortices in a 2D boundary layer, with their structure strongly depending on the sweep angle of the exposed electrode. In the case of zero sweep angle, the strong effect of the spanwise force component at the edges of the MD group on the flow structure is obtained.

The semiemprical model of the actuator section, based on the equivalent force and heat sources, was formulated. The model parameters were determined by the analysis of the flow in quiescent conditions and verified on the vortices structure, induced by the actuator in the boundary layer. Modelling results have shown good coincidence with the experiment in the part of the vortices amplitude and qualitative flow structure, anyhow, the vortex decay rate was overestimated.

The modified actuator model was used to predict the generation of the CF mode in the designed transition delay experiment in T124 wind tunnel in TsAGI. In the linearized approach it was shown that the amplitude of the generated CF mode is within the range required for the transition control by nonlinear modes interaction, at least for this experiment. The amplitude of the initial disturbances, created by the actuator was shown to be below the typical value that can cause the immediate bypass transition.

Acknowledgements

Work is performed within the “BUTERFLI” (BUffet and Transition delay control investigated within European-Russian cooperation for improved FLIght performance) project of the 7th Framework Program of European Commission

References

[1] W. S. Saric, A. L. Carpenter, and H. L. Reed, “Passive control of transition in three-dimensional boundary layers, with emphasis on discrete roughness elements,” *Philos. Trans. R. Soc. A Math. Phys. Eng. Sci.*, vol. 369, no. 1940, pp. 1352–1364, 2011.

[2] P. C. Dörr and M. J. Kloker, “Transition control in a three-dimensional boundary layer by direct attenuation of nonlinear crossflow vortices using plasma actuators,” *Int. J. Heat Fluid Flow*, vol. 61, pp. 449–465, 2016.

[3] S. Chernyshev, A. Kiselev, and A. Kuryachii, “Electrogasdynamic excitation of controlling disturbances near a swept wing leading edge,” vol. 20013, p. 20013, 2016.

[4] P. C. Dörr and M. J. Kloker, “Stabilisation of a three-dimensional boundary layer by base-flow

DOI: 10.13009/EUCASS2017-266

manipulation using plasma actuators," *J. Phys. D. Appl. Phys.*, vol. 48, no. 28, p. 285205, 2015.

[5] J. Serpieri, S. Yadala Venkata, and M. Kotsonis, "Towards laminar flow control on swept wings with AC-DBD plasma actuators as active roughness," in *55th AIAA Aerospace Sciences Meeting*, 2017, p. 1459.

[6] J. Kriegseis, B. Simon, and S. Grundmann, "Towards In-Flight Applications? A Review on Dielectric Barrier Discharge-Based Boundary-Layer Control," *Appl. Mech. Rev.*, vol. 68, no. 2, p. 20802, 2016.

[7] E. Moreau, "Airflow control by non-thermal plasma actuators," *J. Phys. D. Appl. Phys.*, vol. 40, no. 3, pp. 605–636, Feb. 2007.

[8] S. B. Leonov, I. V Adamovich, and V. R. Soloviev, "Dynamics of near-surface electric discharges and mechanisms of their interaction with the airflow," *Plasma Sources Sci. Technol.*, vol. 25, no. 6, p. 63001, 2016.

[9] "Edge effects in flow around a plasma actuator," *Tech. Phys. Lett.*, vol. 43, no. 2, pp. 220–223, 2017.

[10] "The Structure of the Dielectric BarrierDischarge and its Effect on the Discharge Inintiated Gasdynamic Disturbances," in *6th EUCASS*, 2015.

[11] M. Kotsonis, S. Ghaemi, L. Veldhuis, and F. Scarano, "Measurement of the body force field of plasma actuators," *J. Phys. D. Appl. Phys.*, vol. 44, no. 4, p. 45204, 2011.

[12] J. Kriegseis, C. Schwarz, A. Duchmann, S. Grundmann, and C. Tropea, "PIV-based estimation of DBD plasma-actuator force terms," in *50th AIAA Aerospace Sciences Meeting including the New Horizons Forum and Aerospace Exposition*, 2012, no. January, p. AIAA-2012-411.

[13] E. V. Bogdanova and O. S. Ryzhov, "Disturbances in viscouse fluid flow generated by vibrators operating at supercritical frequencies," *Zhurn. Pricl. Math. Techn. Phys.*, no. 4, p. 65–72 (in Russian), 1982.